*J. Fluid Mech.* (2000), *vol.* 422, *pp.* 141–166. Printed in the United Kingdom



# Linear stability analysis of mixed-convection flow in a vertical pipe

By YI-CHUNG SU AND JACOB N. CHUNG†

School of Mechanical and Materials Engineering, Washington State University, Pullman, WA 99164-2920, USA

(Received 1 June 1998 and in revised form 1 March 2000)

A comprehensive numerical study on the linear stability of mixed-convection flow in a vertical pipe with constant heat flux is presented with particular emphasis on the instability mechanism and the Prandtl number effect. Three Prandtl numbers representative of different regimes in the Prandtl number spectrum are employed to simulate the stability characteristics of liquid mercury, water and oil. The results suggest that mixed-convection flow in a vertical pipe can become unstable at low Reynolds number and Rayleigh numbers irrespective of the Prandtl number, in contrast to the isothermal case. For water, the calculation predicts critical Rayleigh numbers of 80 and $-120$ for assisted and opposed flows, which agree very well with experimental values of $Ra_c = 76$ and $-118$ (Scheele & Hanratty 1962). It is found that the first azimuthal mode is always the most unstable, which also agrees with the experimental observation that the unstable pattern is a double spiral flow. Scheele & Hanratty's speculation that the instability in assisted and opposed flows can be attributed to the appearance of inflection points and separation is true only for fluids with $O(1)$ Prandtl number. Our study on the effect of the Prandtl number discloses that it plays an active role in buoyancy-assisted flow and is an indication of the viability of kinematic or thermal disturbances. It profoundly affects the stability of assisted flow and changes the instability mechanism as well. For assisted flow with Prandtl numbers less than 0.3, the thermal–shear instability is dominant. With Prandtl numbers higher than 0.3, the assisted-thermal–buoyant instability becomes responsible. In buoyancy-opposed flow, the effect of the Prandtl number is less significant since the flow is unstably stratified. There are three distinct instability mechanisms at work independent of the Prandtl number. The Rayleigh–Taylor instability is operative when the Reynolds number is extremely low. The opposed-thermal–buoyant instability takes over when the Reynolds number becomes higher. A still higher Reynolds number eventually leads the thermal–shear instability to dominate. While the thermal–buoyant instability is present in both assisted and opposed flows, the mechanism by which it destabilizes the flow is completely different.

## 1. Introduction

Mixed convection is of fundamental and practical interest since most flows are non-isothermal in engineering applications. Mixed convective heat transfer in vertical channels, pipes and annuli has been extensively investigated because of its applications in nuclear reactors, heat exchangers, electronic system cooling, etc. In engineering

† Author to whom correspondence should be sent; current address: Department of Mechanical Engineering, University of Florida, P.O. Box 116300, Gainesville, FL 32611-6300, USA.

analysis, the fully-developed and parallel flow assumptions are often made and hence an analytical laminar solution becomes accessible to facilitate the analysis of heat transfer characteristics. However, the flows that occur in nature not only obey the equations of fluid dynamics, but must also be stable (Landau & Lifshitz 1959). An engineering design, based on laminar solutions which are unstable to ubiquitous disturbances, is treacherous and may produce significant errors.

The stability of an isothermal pipe flow, i.e. the Hagen–Poiseuille flow, is a classical problem and has been investigated by numerous researchers (Fox, Lessen & Bhat 1968; Lessen, Sadler & Liu 1968; Davey & Drazin 1969; Salwen, Cotton & Grosch 1980). All of them reach the same conclusion that isothermal pipe flow is linearly stable, which is at odds with the common observation that pipe flow undergoes transition at a Reynolds number of $O(2000)$. Later theoretical studies indicate that a subcritical instability is a result of finite-amplitude disturbances (Reynolds & Potter 1967; Davey & Nguyen 1971). It is also well known that plane Poiseuille flow is stable to infinitesimal disturbances as long as the Reynolds number is less than 5772 (Orszag 1971). On the other hand, it has been shown that non-isothermal flow instability and transition differ substantially from those of isothermal flow (Gebhart *et al.* 1988). The earliest work on the stability of non-isothermal pipe flow was conducted by, among others, Hanratty, Rosen & Kabel (1958) and Scheele & Hanratty (1962). Based on fully-developed and laminar parallel flow approximations, Hanratty *et al.* (1958) obtained an analytical solution for mixed convection flow in a vertical pipe and observed experimentally that the flow is stable in the entry region but highly unstable after the flow is fully developed. They found that the flow goes through transition at rather low Reynolds numbers. However, instead of becoming turbulent, a new equilibrium flow, which consists of large-scale, regular and periodic motions, was observed. Similar flow patterns have also been observed by Kemeny & Somers (1962) and are called non-laminar flow to distinguish them from turbulent patterns. The striking fact is that such non-isothermal flow can occur at a Reynolds number as low as 30 and the associated heat transfer rates can be 30% larger than those in laminar flow. A significant increase in heat transfer rates above those of laminar flow during low Reynolds number flow transition was also observed by Maitra & Raju (1975) in mixed convection of a heated vertical annulus flow.

Scheele & Hanratty (1962) also reported that for heated upflow (buoyancy assisted), the flow first becomes unstable when the velocity profiles develop points of inflection. The flow is supercritically stable and the transition to turbulence is gradual. For heated downflow (buoyancy opposed), the instability is associated with separation from the wall and the flow is subcritically unstable. Transition is sudden and occurs shortly after the flow becomes unstable. Scheele & Hanratty (1962) observed in their experiment that the flow stability depends primarily on the shape of the velocity profile, which is modified by heating, and the dependence on the Reynolds number is only secondary. Later, El-Genk & Rao (1990) observed similar transition sequences at low Reynolds number for non-isothermal flow in a vertical annulus.

The first theoretical work on the stability of mixed-convection flow was performed by Yao (1987*a*, *b*). He performed a linear stability analysis for the heated pipe flow of water and found that the fully-developed non-isothermal flow is highly unstable. Yao and his group also have reported important work on identifying linear thermal instability in a vertical annulus (Yao & Rogers 1989; Rogers & Yao 1993). Chen & Chung (1996) investigated the same problem in a vertical channel. In essence, all these studies demonstrate two origins of thermal instabilities: shear production and thermal buoyant potential. For buoyancy-assisted flow with constant heat flux, a

sufficiently distorted mean flow profile due to increased heating triggers the instability. Rogers & Yao (1993) called this type of instability thermal–shear instability since the disturbance gains its kinetic energy at the expense of mean-flow kinetic energy through the Reynolds stress. Therefore an inflectional velocity profile due to heating gives rise to an inviscid instability and results in a dramatic reduction in the critical Reynolds number in non-isothermal flow. Rogers & Yao (1993) also discovered a second type of thermal instability, termed thermal–buoyant instability. The thermal–buoyant instability draws its kinetic energy mainly from thermal buoyant potential and exists in higher Prandtl number fluids. For buoyancy-opposed flow, the Rayleigh–Taylor instability prevails unless the Prandtl number is larger than 100 (Yao & Rogers 1989).

The present work intends to offer a comprehensive account of the linear stability features of a non-isothermal vertical pipe flow because of its omni-presence in engineering applications. The stability characteristics of different fluids covering different Prandtl number ranges are investigated with particular emphasis on the instability mechanisms and the role played by the Prandtl number in non-isothermal flow instability through energetics analysis. Different instability mechanisms are identified, some of which are given a new interpretation upon a closer examination. This paper is organized as follows. The formulation of the problem, including the governing equations, non-dimensionalization and base flows, is outlined in § 2. The numerical method employed to solve the stability equations is described in § 3. Results as well as discussion of the numerical solutions are given in § 4. The main conclusions from this study are summarized in § 5.

## 2. Formulation

The problem under study is a fully-developed non-isothermal flow in a vertical pipe with constant heat flux. We non-dimensionalize the length by the radius of the pipe $R_0^*$, the velocity by the centreline axial velocity $W_c^*$ of the isothermal flow, the time by $R_0^*/W_c^*$, the pressure by $\rho^* W_c^{*2}$, where $\rho^*$ is fluid density and let $T^* = T_w^* - C_1^* R_0^* RePr\theta$, wherein $\theta$ is the dimensionless temperature, $C_1^*$ is the axial temperature gradient, $T_w^* = T_{w0}^* + C_1^* R_0^* z$, $T_{w0}^*$ is the reference wall temperature. After so doing and invoking the Boussinesq approximation, the following dimensionless governing equations are reached:

$$\frac{1}{r}\frac{\partial}{\partial r}(ru) + \frac{1}{r}\frac{\partial v}{\partial \phi} + \frac{\partial w}{\partial z} = 0, \tag{2.1}$$

$$\frac{\partial u}{\partial t} + u\frac{\partial u}{\partial r} + \frac{v}{r}\frac{\partial u}{\partial \phi} + w\frac{\partial u}{\partial z} - \frac{v^2}{r} = -\frac{\partial p}{\partial r} + \frac{1}{Re}\left(\nabla^2 u - \frac{u}{r^2} - \frac{2}{r^2}\frac{\partial v}{\partial \phi}\right), \tag{2.2}$$

$$\frac{\partial v}{\partial t} + u\frac{\partial v}{\partial r} + \frac{v}{r}\frac{\partial v}{\partial \phi} + w\frac{\partial v}{\partial z} + \frac{uv}{r} = -\frac{1}{r}\frac{\partial p}{\partial \phi} + \frac{1}{Re}\left(\nabla^2 v - \frac{v}{r^2} + \frac{2}{r^2}\frac{\partial u}{\partial \phi}\right), \tag{2.3}$$

$$\frac{\partial w}{\partial t} + u\frac{\partial w}{\partial r} + \frac{v}{r}\frac{\partial w}{\partial \phi} + w\frac{\partial w}{\partial z} = -\frac{\partial p}{\partial z} - \frac{Ra}{Re}\theta + \frac{1}{Re}\nabla^2 w, \tag{2.4}$$

$$\frac{\partial \theta}{\partial t} + u\frac{\partial \theta}{\partial r} + \frac{v}{r}\frac{\partial \theta}{\partial \phi} + w\frac{\partial \theta}{\partial z} = \frac{w}{RePr} + \frac{1}{RePr}\nabla^2\theta, \tag{2.5}$$

where the dimensionless parameters are the Reynolds number, $Re = W_c^* R_0^*/\nu^*$, the Rayleigh number, $Ra = g^*\beta^* C_1^* R_0^{*4}/\nu^*\kappa^*$, which is positive for heating and negative for cooling, and the Prandtl number, $Pr = \nu^*/\kappa^*$, and $\nabla^2$ is the Laplacian in the

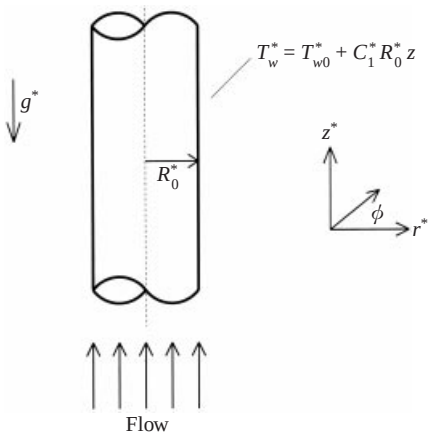


FIGURE 1. Schematic of vertical pipe flow and the coordinate system.

cylindrical coordinates. The symbols appearing in the dimensionless groups are $\nu^*$ for momentum diffusivity, $g^*$ for the gravity pointing in the negative $z$-direction, $\beta^*$ for thermal expansion coefficient and $\kappa^*$ for thermal diffusivity. The pressure work and dissipation in the energy equation have been dropped due to the moderate flow velocity in the present analysis. Therefore, in the present problem, the system is governed by the parameter triad $(Re, Ra, Pr)$ as in many flow systems involved with mixed convection. The Reynolds number is a measure of the influence of forced convection while the Rayleigh number represents the natural convection effect. The Prandtl number plays a somewhat different role in non-isothermal flow stability than it does in traditional heat transfer problems, as we shall see later. The schematic of the flow system investigated is given in figure 1.

Since we will compare our numerical results with the experimental measurement of Scheele & Hanratty (1962), a relationship between the dimensionless parameters used in their study and this work is needed. Scheele & Hanratty represented the heating level by the group $G/R$, where $G = R_0^{*4}\beta^* g^* q^*/k^* \nu^{*2}$ and $R = \bar{W} R_0^*/\nu^*$, with $\bar{W}$ the average velocity, $k^*$ the thermal conductivity and $q^*$ the wall heat flux. Their $q^*$ is related to our $C_1^*$ by $C_1^* = -q^*/k^* RePr\Theta'(1)$. It can be readily verified that $G/R = -2Ra\Theta'(1) = Ra/2$. Thus, the group $G/R$ Scheele & Hanratty employed to represent the level of heating is half the value of the Rayleigh number adopted herein.

In accordance with the linear stability theory, the laminar solutions are perturbed by infinitesimal disturbances. To this end, the flow variables are decomposed into a laminar part plus an infinitesimal perturbation and then substituted into the governing equations. Neglecting the nonlinear terms and decomposing perturbations into the normal modes, i.e. $u' = \hat{u}(r)\exp\{i\alpha(z - ct) + in\phi\}$ and similar expressions for other variables, yields the linear stability equations

$$\frac{d\hat{u}}{dr} + \frac{\hat{u}}{r} + \frac{in}{r}\hat{v} + i\alpha\hat{w} = 0, \tag{2.6}$$

$$\frac{d^2\hat{u}}{dr^2} + \left(\frac{1}{r} - ReU\right)\frac{d\hat{u}}{dr} + \left(\frac{i^2n^2}{r^2} + i^2\alpha^2 - \frac{1}{r^2} - Re\frac{dU}{dr} - \frac{inRe}{r}V - i\alpha ReW + i\alpha cRe\right)\hat{u} + \left(-\frac{2in}{r^2} - \frac{2Re}{r}V\right)\hat{v} - Re\frac{d\hat{p}}{dr} = 0, \tag{2.7}$$

$$\left(-\frac{Re}{r}V+\frac{2in}{r^2}-Re\frac{\mathrm{d}V}{\mathrm{d}r}\right)\hat{u}+\frac{\mathrm{d}^2\hat{v}}{\mathrm{d}r^2}+\left(\frac{1}{r}-ReU\right)\frac{\mathrm{d}\hat{v}}{\mathrm{d}r}$$
$$+\left(\frac{\mathrm{i}^2n^2}{r^2}+\mathrm{i}^2\alpha^2-\frac{1}{r^2}-\frac{inRe}{r}V-\mathrm{i}\alpha ReW-\frac{Re}{r}U+\mathrm{i}\alpha cRe\right)\hat{v}-\frac{inRe}{r}\hat{p}=0, \quad (2.8)$$

$$-Re\frac{\mathrm{d}W}{\mathrm{d}r}\hat{u}+\frac{\mathrm{d}^2\hat{w}}{\mathrm{d}r^2}+\left(\frac{1}{r}-ReU\right)\frac{\mathrm{d}\hat{w}}{\mathrm{d}r}$$
$$+\left(\frac{\mathrm{i}^2n^2}{r^2}+\mathrm{i}^2\alpha^2-\frac{inRe}{r}V-\mathrm{i}\alpha ReW+\mathrm{i}\alpha cRe\right)\hat{w}-\mathrm{i}\alpha Re\hat{p}-Ra\hat{\theta}=0, \quad (2.9)$$

$$-RePr\frac{\mathrm{d}\Theta}{\mathrm{d}r}\hat{u}+\hat{w}+\frac{\mathrm{d}^2\hat{\theta}}{\mathrm{d}r^2}+\left(\frac{1}{r}-RePrU\right)\frac{\mathrm{d}\hat{\theta}}{\mathrm{d}r}$$
$$+\left(\frac{\mathrm{i}^2n^2}{r^2}+\mathrm{i}^2\alpha^2-\frac{inRePr}{r}V-\mathrm{i}\alpha RePrW+\mathrm{i}\alpha cRePr\right)\hat{\theta}=0. \quad (2.10)$$

The boundary conditions accompanying the above equations are specified at the wall and the centre. At the wall, all the disturbances must vanish. This implies

$$\hat{u}=\hat{v}=\hat{w}=\frac{\mathrm{d}\hat{p}}{\mathrm{d}r}=\hat{\theta}=0, \quad r=1. \quad (2.11a)$$

At the pipe centreline, the boundary conditions are as follows (Khorrami, Malik & Ash 1989):

$$\left.\begin{array}{ll}\hat{u}=\hat{v}=\mathrm{d}\hat{w}/\mathrm{d}r=\mathrm{d}\hat{p}/\mathrm{d}r=\mathrm{d}\hat{\theta}/\mathrm{d}r=0, & r=0,\ n=0,\\ \hat{u}+\mathrm{i}\hat{v}=2\mathrm{d}\hat{u}/\mathrm{d}r+\mathrm{i}\mathrm{d}\hat{v}/\mathrm{d}r=\hat{w}=\hat{p}=\hat{\theta}=0, & r=0,\ n=1,\\ \hat{u}=\hat{v}=\hat{w}=\hat{p}=\hat{\theta}=0, & r=0,\ n\geqslant 2.\end{array}\right\} \quad (2.11b)$$

The stability or instability of the laminar flow is determined by the sign of the eigenvalue $c$. In solving (2.6)–(2.11), the traditional approach is to eliminate the pressure term to reduce the number of governing equations. The primitive variable formulation of the governing equations, as introduced by Khorrami *et al.* (1989), is adopted herein. As pointed out by Khorrami *et al.*, although this formulation requires somewhat higher computer storage, the advantage is that it is easily adaptable to various flow situations like pipe flow, annulus flow, rotating pipe flow and a trailing line vortex. Besides, this formulation can be easily used to solve spatial stability problems by a companion matrix method.

Two cases of laminar base flow will be investigated. The first one is an upward flow with constant flux heating. Such mixed convection is also called buoyancy assisted since the buoyancy force acts in the direction of the forced flow. The other case is an upward flow with constant flux cooling and is termed buoyancy-opposed flow. Because equations (2.6)–(2.11) are invariant under the transformation $(W, w', \Theta, \theta', z) \rightarrow (-W, -w', -\Theta, -\theta', -z)$, the stability characteristics of a heated upward flow are identical to those of a cooled downward flow and a cooled upward flow is equivalent to a heated downward flow insofar as stability is concerned.

Under constant-flux and fully-developed assumptions, the laminar velocity and temperature profiles of buoyancy assisted and opposed flows are given below.

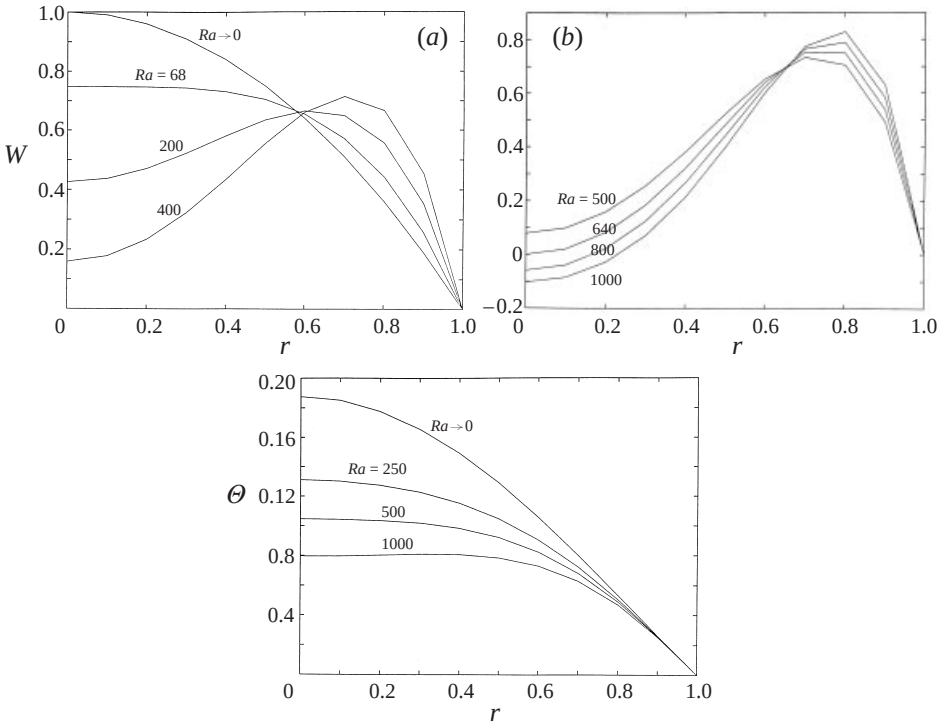


FIGURE 2. Velocity profiles of assisted flow for (*a*) $Ra \leqslant 400$, and (*b*) $Ra \geqslant 400$. (*c*) Temperature profiles of assisted flow.

*Laminar base flow* (*A*): *buoyancy-assisted flow*

In this case, the mean flow solution is (Hanratty *et al.* 1958)

$$\left.\begin{aligned} U(r) &= V(r) = 0, \\ W(r) &= c_1 \mathrm{ber}(rRa^{1/4}) + c_2 \mathrm{bei}(rRa^{1/4}), \\ \Theta(r) &= -Ra^{-1/2}(c_1\{\mathrm{bei}(rRa^{1/4}) - \mathrm{bei}(Ra^{1/4})\} - c_2\{\mathrm{ber}(rRa^{1/4}) - \mathrm{ber}(Ra^{1/4})\}), \end{aligned}\right\} \tag{2.12}$$

where

$$c_1 = \frac{0.25Ra^{1/4}\mathrm{bei}(Ra^{1/4})}{\mathrm{ber}'(Ra^{1/4})\mathrm{ber}(Ra^{1/4}) + \mathrm{bei}'(Ra^{1/4})\mathrm{bei}(Ra^{1/4})}, \tag{2.13a}$$

$$c_2 = \frac{-c_1 \mathrm{ber}(Ra^{1/4})}{\mathrm{bei}(Ra^{1/4})}, \tag{2.13b}$$

and

$$\mathrm{ber}(x) + \mathrm{i}\,\mathrm{bei}(x) = J_0\left(\frac{-1+\mathrm{i}}{\sqrt{2}}x\right)$$

are the Kelvin functions, $\mathrm{i} = \sqrt{-1}$, and $J_0$ is the Bessel function of the first kind of order zero.

According to (2.12), the velocity and temperature profiles are not a direct function of the Prandtl number and the Reynolds number, a consequence of the fully-developed

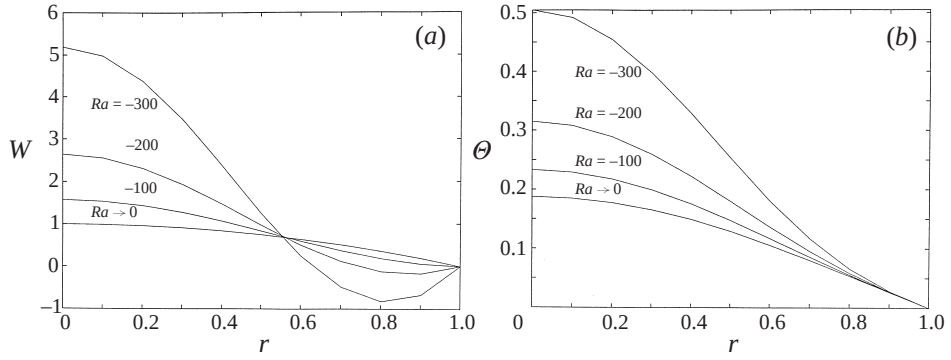


FIGURE 3. (*a*) Velocity profiles and (*b*) temperature profiles of opposed flow.

assumption, but depend solely on the Rayleigh number. The velocity and temperature profiles of buoyancy-assisted flow at different Rayleigh numbers are plotted in figure 2 to illustrate the distortion from isothermal distributions due to different heating levels. Velocity profiles for $Ra \to 0$, $Ra = 68, 200, 400$ are shown in figure 2(*a*) while those for $Ra = 500, 640, 800$ and 1000 are given in figure 2(*b*). The common feature of the effect of heating on the isothermal parabolic profile is that the fluid near the wall moves faster due to heating and the fluid motion near the pipe centre is retarded in order to satisfy the global mass conservation imposed by a pump or other means. Note that once $Ra \geqslant 68$, the velocity profile develops an inflection point near the pipe centre and in accordance with the stability theory (Drazin & Reid 1981), the flow is inviscidly unstable. Furthermore, for $Ra \geqslant 640$, reversal of flow occurs near the pipe centre, as shown in figure 2(*b*). Figure 2(*c*) depicts the laminar temperature profiles for $Ra \to 0$, $Ra = 250, 500$ and 1000. Due to the form of the non-dimensionalization, the temperature profiles for heating do not deviate much from that of an isothermal flow. The wall temperature gradient $\Theta'(1)$ remains $-1/4$ since the heat flux is constant.

*Laminar base flow* (*B*): *buoyancy-opposed flow*

For opposed flow, the base flow solution is (Hanratty *et al.* 1958)

$$\left.\begin{aligned} &U(r) = V(r) = 0, \\ &W(r) = c_3 J_0\{r(-Ra)^{1/4}\} + c_4 I_0\{r(-Ra)^{1/4}\}, \\ &\Theta(r) = (-Ra)^{1/2}(c_3\{J_0\{r(-Ra)^{1/4}\} - J_0\{(-Ra)^{1/4}\}\} \\ &\qquad -c_4\{I_0\{r(-Ra)^{1/4}\} - I_0\{(-Ra)^{1/4}\}\}), \end{aligned}\right\} \tag{2.14}$$

where

$$c_3 = \frac{0.25(-Ra)^{1/4} I_0\{(-Ra)^{1/4}\}}{I_0\{(-Ra)^{1/4}\} J_1\{(-Ra)^{1/4}\} - J_0\{(-Ra)^{1/4}\} I_1\{(-Ra)^{1/4}\}} \tag{2.15a}$$

and

$$c_4 = \frac{-c_3 J_0\{(-Ra)^{1/4}\}}{I_0\{(-Ra)^{1/4}\}}. \tag{2.15b}$$

$J_1$ is the Bessel function of the first kind of order one, $I_0$ and $I_1$ the Bessel functions of the second kind of order zero and one, respectively.

Figure 3 illustrates the velocity and temperature profiles for opposed flow. In contrast to the case for assisted flow, the fluid moves faster in the central portion and

slower near the wall in opposed flow. The flow also develops an inflection point near the wall at $Ra < -19.7$ and separation occurs at a Rayleigh number equal to about $-105$. After separation, reversal of flow occurs near the pipe wall.

For the constant wall temperature case, Rosen & Hanratty (1961) used boundary layer theory to show that at the location of maximum profile distortion, the velocity and temperature fields could be described by equations similar to (2.12)–(2.15). As a consequence, the stability features presented in § 4 are also applicable qualitatively to a heated vertical pipe with constant wall temperature.

## 3. Method of solution

The Chebyshev collocation method (Canuto *et al.* 1988) is employed to solve the linearized disturbance equations. In the collocation method, the collocation points are chosen as

$$x_j = \cos\frac{\pi j}{N}, \quad j = 0, 1, 2, \ldots, N. \tag{3.1}$$

The unknown function $f(x)$ and its derivatives are expressed in terms of the values of that function at the collocation points

$$\frac{\mathrm{d}^k f}{\mathrm{d}x^k}(x_j) = \sum_{i=0}^{N} (D_N)_{ji}^k f(x_i), \quad j = 0, 1, \ldots, N, \tag{3.2}$$

where

$$(D_N)_{ji} = \begin{cases} \bar{c}_j(-1)^{j+i}/\bar{c}_i(x_j - x_i), & j \neq i, \\ -x_i/2(1-x_i)^2, & 1 \leqslant j = i \leqslant N-1, \\ (2N^2+1)/6, & j = i = 0, \\ (-2N^2+1)/6, & j = i = N. \end{cases} \tag{3.3}$$

The collocation approximation to the governing equations and boundary conditions is to enforce (2.6)–(2.10) at $x_j, j = 1, \ldots, N-1$ and (2.11) at $x_j, j = 0$ and $N$. Since the physical domain is [0,1] while the Chebyshev polynomials are defined in the interval $[-1, 1]$, a linear mapping $x = 1 - 2r$ is used.

Due to the boundary conditions, matrices $\boldsymbol{A}$ and $\boldsymbol{B}$ are singular. A method based on row operations proposed by Gary & Helgason (1970) is used to make $\boldsymbol{A}$ and $\boldsymbol{B}$ non-singular. Then the transformed generalized eigenvalue system is solved using the IMSL subroutine DGVCGG, which originates from a complex QR algorithm by Moler & Stewart (1973), to obtain the eigenvalue spectra and eigenvectors.

## 4. Results and discussion

### 4.1. *Code verification*

To verify the code, we first test it for the isothermal case. The governing equations without the energy equation are solved and the eigenvalues obtained are found to agree well with those documented by Salwen *et al.* (1980). For the non-isothermal case, the solution generated by the code is in excellent agreement with that from our other code, which utilizes the Galerkin weak formulation based on shifted Jacobi polynomials (Su *et al.* 2000). Therefore the validity of the code utilized to generate all the results discussed below is established.

Table 1 illustrates the convergence of the Chebyshev collocation method. At $Re = Ra = 100$, $\alpha = n = 1$, 13 terms of Chebyshev polynomials achieve 5-digit point

| $N$ (terms) | Most unstable mode |
|---|---|
| 7 | 0.7283168514 + 0.02373105009i |
| 10 | 0.7286739735 + 0.02385607831i |
| 11 | 0.7286646507 + 0.02384154284i |
| 13 | 0.7286654210 + 0.02384030212i |
| 15 | 0.7286656404 + 0.02384045018i |
| 17 | 0.7286654854 + 0.02384052103i |
| 19 | 0.7286654227 + 0.02384054452i |
| 21 | 0.7286653857 + 0.02384056145i |
| 25 | 0.7286653473 + 0.02384057883i |
| 31 | 0.7286653252 + 0.02384058905i |
| 40 | 0.7286653029 + 0.02384059972i |
| 50 | 0.7286653063 + 0.02384059802i |
| 60 | 0.7286653075 + 0.02384059739i |
| 70 | 0.7286653081 + 0.02384059716i |

TABLE 1. Convergence of the Chebyshev collocation method, $Re = 100$, $Ra = 100$, $Pr = 7$, $n = 1$, $\alpha = 1$.

accuracy. As the number of terms increases, the results remain consistent and the accuracy improves as well. Similar satisfactory results are obtained when the values of the parameters are varied. In the light of the results shown in table 1, it is believed that 50 terms of Chebyshev polynomials are enough to yield very accurate solutions. Thus the results presented below are produced with 50 terms of Chebyshev polynomials.

### 4.2. *Significance of the Prandtl number*

Before addressing the stability of heated pipe flow, we should first examine the role played by the Prandtl number in non-isothermal flow stability problems. To illustrate this, we solve the governing equations with a vanishingly small Rayleigh number ($Ra \rightarrow 0$) and various Prandtl numbers. This corresponds to an almost isothermal flow subject to velocity (kinetic) and temperature (thermal) perturbations. Five different Prandtl numbers, 0.01, 0.1, 1.0, 10 and 100, are used. The first ten least-stable eigenvalues of nearly isothermal flow with different orders of Prandtl numbers at a Reynolds number of 100 are given in table 2. By comparing the spectra with those obtained without solving the energy equation, each mode can be classified as a kinetic mode or a thermal mode as the letter K or T signifies in table 2. For a Prandtl number as low as 0.01, all ten modes are kinetic in nature. On the other hand, at a Prandtl number of 100, nine out of ten least-stable modes are thermal modes. When the Prandtl number is unity, there are three thermal modes (the 2nd, 4th and 8th, respectively). At other large Reynolds numbers like 4000 and 9600, the spectra exhibit similar behaviour. This prompt us to probe the role played by the Prandtl number in non-isothermal stability. The answer can be found by examining diffusion terms in the momentum equations (2.2)–(2.4) and the energy equation (2.5). In momentum equations, the reciprocal of the Reynolds number measures the importance of momentum diffusion whereas $(RePr)^{-1}$ indicates the magnitude of thermal diffusion. Thus, in mixed convection, the Prandtl number reveals the relative efficiency of momentum diffusion and thermal diffusion. If the Prandtl number is much less than $O(1)$, say 0.01, thermal fluctuations will be quickly smoothed out and all the least-stable modes are induced by kinetic disturbances. On the other hand, when the Prandtl number is much greater than $O(1)$, the thermal modes survive. When the Prandtl number is of $O(1)$, these two modes compete against each other.

| Mode | $Pr = 0.01$ | Type | $Pr = 0.1$ | Type | $Pr = 1.0$ | Type | $Pr = 10.0$ | Type | $Pr = 100.0$ | Type |
|---|---|---|---|---|---|---|---|---|---|---|
| 1 | $0.57256 - 0.14713i$ | K | $0.57256 - 0.14713i$ | K | $0.57256 - 0.14713i$ | K | $0.91005 - 0.09044i$ | T | $0.97171 - 0.02838i$ | T |
| 2 | $0.55198 - 0.37446i$ | K | $0.55198 - 0.37446i$ | K | $0.68626 - 0.27345i$ | T | $0.57256 - 0.14713i$ | K | $0.94343 - 0.05666i$ | T |
| 3 | $0.78735 - 0.47946i$ | K | $0.78735 - 0.47946i$ | K | $0.55198 - 0.37446i$ | K | $0.31216 - 0.17055i$ | T | $0.14721 - 0.08279i$ | T |
| 4 | $0.66247 - 0.74907i$ | K | $0.66247 - 0.74907i$ | K | $0.64647 - 0.45937i$ | T | $0.82110 - 0.17989i$ | T | $0.91514 - 0.08495i$ | T |
| 5 | $0.66884 - 1.00009i$ | K | $0.66884 - 1.00009i$ | K | $0.78735 - 0.47946i$ | K | $0.73084 - 0.26820i$ | T | $0.88686 - 0.11323i$ | T |
| 6 | $0.67804 - 1.36860i$ | K | $0.67804 - 1.36860i$ | K | $0.66247 - 0.74907i$ | K | $0.53431 - 0.27222i$ | T | $0.25481 - 0.13980i$ | T |
| 7 | $0.66074 - 1.75359i$ | K | $0.66676 - 1.57781i$ | T | $0.66884 - 1.00009i$ | K | $0.67301 - 0.34717i$ | T | $0.85858 - 0.14152i$ | T |
| 8 | $0.67703 - 2.20188i$ | K | $0.66074 - 1.75359i$ | K | $0.66663 - 1.02767i$ | T | $0.55198 - 0.37446i$ | K | $0.57256 - 0.14713i$ | K |
| 9 | $0.66151 - 2.69704i$ | K | $0.67703 - 2.20188i$ | K | $0.67804 - 1.36860i$ | K | $0.78735 - 0.47946i$ | K | $0.83037 - 0.16955i$ | T |
| 10 | $0.67467 - 3.23690i$ | K | $0.66151 - 2.69704i$ | K | $0.66074 - 1.75359i$ | K | $0.67190 - 0.48060i$ | T | $0.34131 - 0.18317i$ | T |

TABLE 2. The first 10 eigenmodes for isothermal flow with different Prandtl numbers, $Re = 100$, $n = 1$, $\alpha = 1$. K denotes a kinetic mode and T a thermal mode.

As a result, in non-isothermal flow stability, the order of the Prandtl number provides a clue to whether kinetic or thermal perturbations may be sustained. The dominant modes for assisted and opposed flows at various combinations of $(Re, Ra, Pr, \alpha, n)$ are documented in detail by Su (1994).

### 4.3. *Energetics of disturbances*

To shed some light on the mechanism leading to the instability, an investigation of the energy budget of the disturbances is made so that the energy transfer between the mean flow and the disturbances can be presented and the underlying physics can be explored. To this end, the equations governing the energy balance of the disturbances are derived and given as follows:

$$\frac{\partial}{\partial t}\iiint_V E_k \,\mathrm{d}V = \underbrace{\iiint_V -u'w'\frac{\mathrm{d}W}{\mathrm{d}r}\,\mathrm{d}V}_{\mathrm{E_S}} \underbrace{-\frac{1}{Re}\iiint_V (\xi'^2+\eta'^2+\zeta'^2)\,\mathrm{d}V}_{\mathrm{E_D}} \underbrace{-\frac{Ra}{Re}\iiint_V \boldsymbol{u}'\cdot(\theta'\boldsymbol{e}_z)\,\mathrm{d}V}_{\mathrm{E_B}}, \tag{4.1}$$

$$\frac{\partial}{\partial t}\iiint_V E_\theta \,\mathrm{d}V = \underbrace{-\iiint_V \theta'u'\frac{\mathrm{d}\Theta}{\mathrm{d}r}\,\mathrm{d}V}_{\mathrm{E_T}} \underbrace{+\frac{1}{RePr}\iiint_V w'\theta'\,\mathrm{d}V}_{(RaPr^{-1})\,\mathrm{E_B}} \underbrace{-\frac{1}{RePr}\iiint_V |\nabla\theta'|^2 \mathrm{d}V}_{\mathrm{E_C}}, \tag{4.2}$$

where $E_k = \frac{1}{2}\boldsymbol{u}'\cdot\boldsymbol{u}'$, $E_\theta = \frac{1}{2}\theta'^2$ are the disturbance kinetic energy and thermal variance, respectively, and $\xi', \eta'$ and $\zeta'$ are the disturbance vorticity in the $r$-, $\theta$- and $z$-directions, respectively. The integration is carried out over the volume of one disturbance wave with wavelength $\lambda_z$, so $V \equiv \{(r,\theta,z) \mid r \in [0,1], \theta \in [0,2\pi], z \in [0,\lambda_z]\}$.

In equation (4.1), the first term on the right-hand side, denoted by $\mathrm{E_S}$, represents the gain/loss of disturbance kinetic energy from/to the mean flow through the Reynolds stress. It is called the shear production (destruction). The second term, denoted by $\mathrm{E_D}$, is a negative definite quantity representing the dissipation of disturbance kinetic energy through the viscous effect. It can be seen that the viscosity plays a dual role: it may destabilize the flow through the Reynolds stress but always stabilizes the flow through the effect of viscous dissipation. The last term, denoted by $\mathrm{E_B}$, due to the non-isothermal effect, represents the production (destruction) of disturbance kinetic energy through the buoyancy effect and is called the buoyant production (destruction). Therefore (4.1) contains the rate of change of disturbance kinetic energy due to the interplay of the shear, dissipation and buoyancy effects.

In equation (4.2), the first term on the right-hand side, denoted by $\mathrm{E_T}$, is the gradient production (destruction) of the thermal variance via the mean-flow temperature gradient. This term plays the same role as the shear production term $\mathrm{E_S}$ does in (4.1). The second term represents the exchange of kinetic and thermal disturbance energy due to the buoyant force and is the negative of the buoyant production in (4.1) divided by $RaPr$. Consequently this term represents the transfer of energy between kinetic disturbances and thermal disturbances through buoyancy. The last term in (4.2), denoted by $\mathrm{E_C}$, is the dissipation of thermal variance due to thermal conduction and is analogous to $\mathrm{E_D}$ in (4.1). So (4.2) is the balance of thermal variance due to the effects of gradient production, transfer of energy between the kinetic and thermal disturbances, and conduction dissipation.

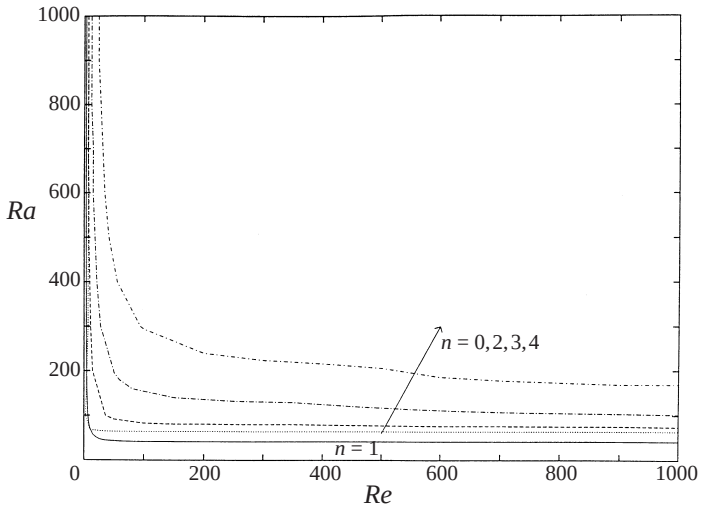


FIGURE 4. Stability map of assisted flow for oil, $Pr = 100$.

On the neutral stability curve, the disturbances neither amplify nor decay. Hence the left-hand sides of (4.1) and (4.2) vanish. The disturbance field variables are the eigenvectors from the linear stability analysis. The integrals in (4.1) and (4.2) are evaluated by Gauss–Chebyshev quadratures (Abramowitz & Stegun 1972).

### 4.4. *Buoyancy-assisted flow stability*

In our numerical calculations, three Prandtl numbers, 0.0248, 7 and 100 are selected to simulate the stability characteristics of liquid mercury, water and oil, respectively. It is believed that these three Prandtl numbers represent well the Prandtl number spectrum for liquid metals, most liquids and heavy oils.

The stability boundary of various azimuthal wavenumbers for oil is shown in figure 4. The first notable feature is that the first azimuthal mode is the most unstable. The unstable flow pattern is a double spiral wave, which agrees with the experimental observation of Scheele & Hanratty (1962). The second common feature of the stability curves is that they have an L shape, with basically vertical lines at low Reynolds numbers that turn mostly horizontal at higher Reynolds numbers. The stability curves depend primarily on the Rayleigh number and the Prandtl number and the dependence on the Reynolds number is secondary. At very low Reynolds numbers, the flow is always stable no matter how high the Rayleigh number is. This is because the fluid is stably stratified in the vertical direction when there is no motion. At low Reynolds numbers, a high heating level, or equivalently a large Rayleigh number, is required to cause instability. But as the Reynolds number is further increased, the critical Rayleigh number decreases drastically and then approaches an asymptotical value. Similar curves are also found for water and liquid mercury except for that the values of the Reynolds number at the turning point and the asymptotic critical Rayleigh number are different (Su 1994). For water and oil, the flow can become unstable at Reynolds numbers as low as 60 and 20 when the Rayleigh numbers exceed 80 and 52, respectively. Scheele & Hanratty (1962) reported that for upflow heating using water as the working fluid, their results on transition asymptotically approach a $G/R$ limit of 42.5 ($Ra = 85$) and 33($Ra = 66$) if the fluid properties are evaluated at the outlet and inlet temperature respectively. They also mentioned that for assisted

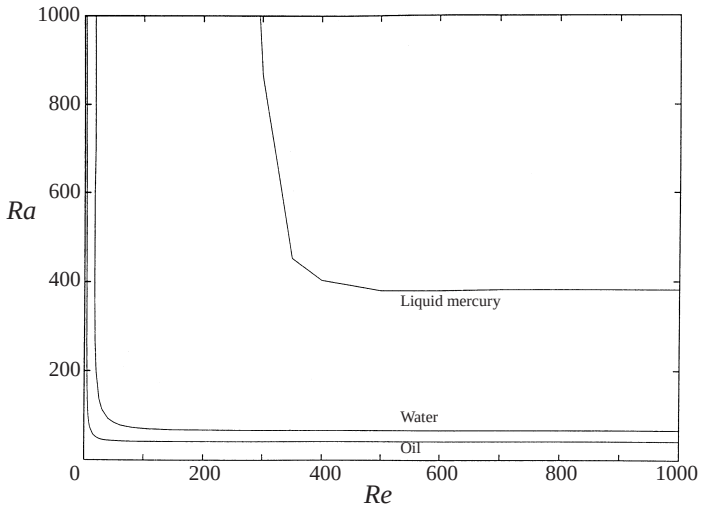


FIGURE 5. Stability map of assisted flow with different Prandtl numbers.

flow, at $G/R = 45(Ra = 90)$, the temperature fluctuations are low-frequency small-scale oscillations, which indicates that their interpretation of transition appears to be onset of instability. Thus, their data on the critical Rayleigh number are in close agreement with our theoretical prediction.

These results show that non-isothermal flow can develop instability at a low speed under mild heating levels. This is surprisingly different from an isothermal pipe flow since the latter is unconditionally stable to infinitesimal disturbances ($Re_c = \infty$). The reason why assisted flow becomes unstable at low Reynolds number is that a slow flow can carry denser fluid upward into the region of lighter fluid under the heating condition, as pointed out by Yao (1987). Since the denser fluid will carry its inertia when it moves into the region of lighter fluid which has a higher velocity, an inflection point develops and a locally high-shear layer appears. This is similar to the 'lift-up' mechanism in the boundary layer in the presence of streamwise vortices (Landahl 1975). Such an effect results in a very dramatic reduction in the critical Reynolds number from infinity in an isothermal flow to less than $O(100)$ in non-isothermal flow. When the convection effect becomes stronger, more denser fluid can be transported upward to destabilize the flow, hence the critical Rayleigh number decreases. However, when the Reynolds number is higher than a certain value, further increase will no longer result in the convection effect to destabilize the flow and the critical Rayleigh number approaches a constant value.

Figure 5 plots the stability map for the chosen fluids to illustrate the effect of the Prandtl number. It is seen that the Prandtl number plays a significant role in the stability characteristics. A higher Prandtl number results in a lower critical Rayleigh number, that is the effect of the Prandtl number is destabilizing. As discussed in § 4.2, for a low Prandtl number fluid, the conduction effect is very strong that any thermal fluctuations in the flow field will be quickly damped out. On the other hand, when the Prandtl number increases, the thermal fluctuations cannot be smoothed out by conduction and remain localized. In assisted flow, the instability is triggered when the denser fluid is carried upward into regions of lighter fluid: apparently the higher the Prandtl number, the more likely it is that the thermal fluctuations remain undamped. Consequently a local disruption of the buoyant force induced by thermal fluctuations

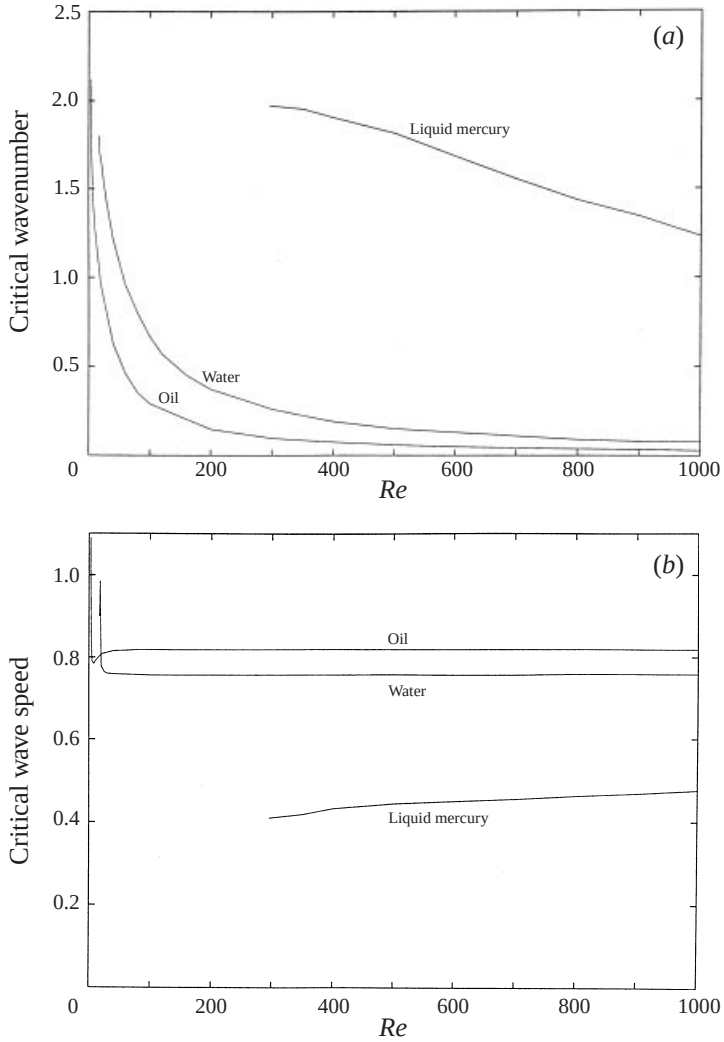


FIGURE 6. (*a*) Critical wavenumber and (*b*) critical wave speed of assisted flow.

will have a better chance of causing the distortion of the velocity field to initiate the instability. With this line of reasoning, it is easy to understand why in an assisted flow the Prandtl number plays a major role in destabilizing the flow. The effect of the Prandtl number will become more transparent when we later study the energetics of the disturbances.

Figure 6 illustrate the variation of the critical axial wavenumber and wave speed with the Reynolds number. For water and oil, the wavenumber along the vertical portion of the stability curve is about 1.75, which corresponds to 3.59 pipe radii. As the Reynolds number is increased, the wavenumber decreases monotonically with the Reynolds number. At $Re = 1000$, the wavenumber drops to about 0.1 for water and oil, corresponding to 62.8 pipe radii, thus the instability wave is relatively much longer. The critical wave speed is insensitive to the Reynolds number and remains almost constant. The variation of the growth rate with different levels of heating is displayed in figure 7. Figure 7(*a*) is the evolution of the disturbance growth rate with

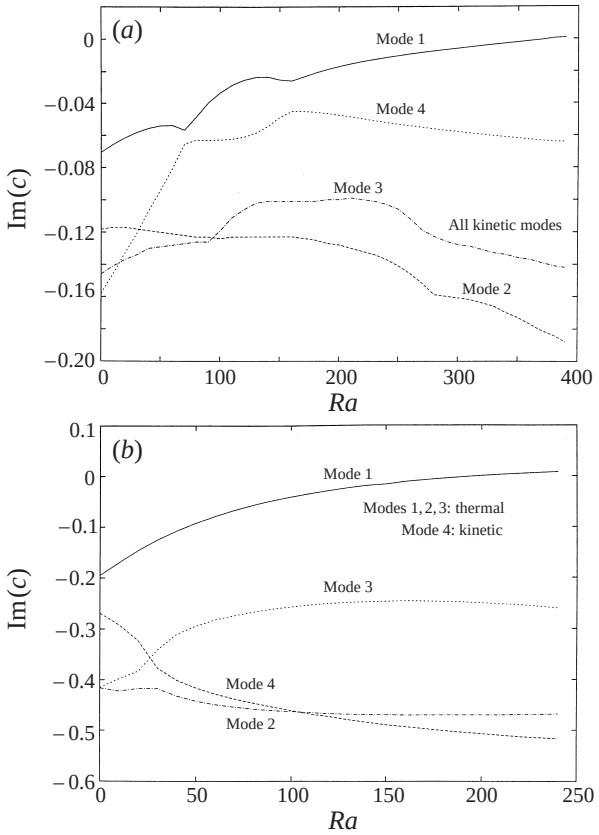


FIGURE 7. Evolution of growth rate with $Ra$ for ($a$) liquid mercury, assisted flow, $Re = 500$, $\alpha = 1.8$ ($b$) water, assisted flow, $Re = 20$, $\alpha = 1.68$.

the Rayleigh number for liquid mercury at $Re = 500$, $\alpha = 1.8$. In this case, the first four least-stable modes are triggered by velocity fluctuations. Figure 7($b$) shows the same evolution diagram for water at $Re = 20$, $\alpha = 1.68$. For water the most unstable modes are induced by thermal fluctuations. Similar results for oil demonstrate that the leading unstable modes are thermal modes and the first kinetic mode is the 13th mode for $Re = 500$ and the 12th mode for $Re = 5$ (Su 1994).

To elucidate the underlying instability mechanisms for the assisted flow, use is made of equation (4.1). The budget for the disturbance kinetic energy is presented in figure 8. Figure 8($a$) gives the energy budget for liquid mercury. It is found that the kinetic disturbances obtain their energy from the mean flow exclusively by shear production. The buoyant production is negative, that is the buoyancy force acts to stabilize the flow. This is anticipated since the flow is stably stratified, and for liquid mercury the Prandtl number is so low that thermal fluctuations are not viable. Therefore the instability mechanism for liquid mercury is termed *thermal–shear* instability. Here *thermal* is used to highlight that the thermal effect modifies the stable parabolic profile and results in an unstable inflectional distribution. The word *shear* underscores the fact that the disturbance kinetic energy is fed by shear production. This instability is hydrodynamic in origin, i.e. due to velocity perturbations in the flow field. Figures 8($b$) and 8($c$) show the energy budgets for water and oil. Opposite to the case for liquid mercury, the disturbances sustain themselves through buoyant

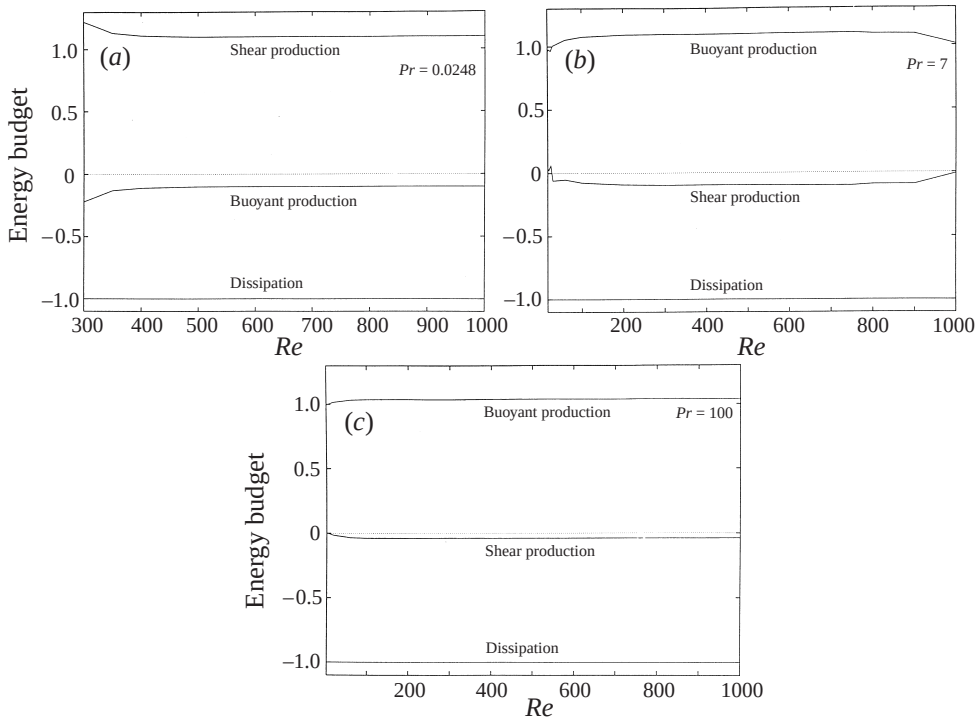


FIGURE 8. Assisted-flow disturbance kinetic energy budget for (*a*) liquid mercury, (*b*) water, (*c*) oil.

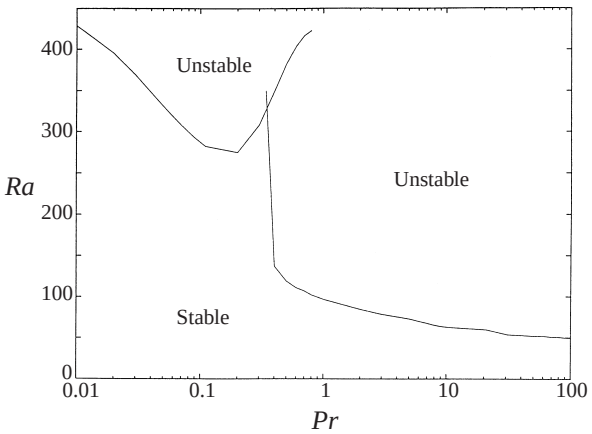


FIGURE 9. Stability map in $Pr, Ra$-space for assisted flow, $Re = 1000$.

production. In this regard, the instability for water and oil is called *assisted-thermal–buoyant* instability: *thermal* is used to account for the fact that the instability is due to undamped thermal perturbations, *buoyant* denoting that the instability is driven by the buoyant production. Since there also exists another type of thermal–buoyant instability in opposed flow but of a different origin, the adjective *assisted* is added. The assisted-thermal–buoyant instability occurs only at higher Prandtl numbers and is more sensitive to the thermal effect. This is further illuminated in figures 9 and 10. Figure 9 is the stability map in the $Pr, Ra$-space for assisted flow with $Re = 1000$,

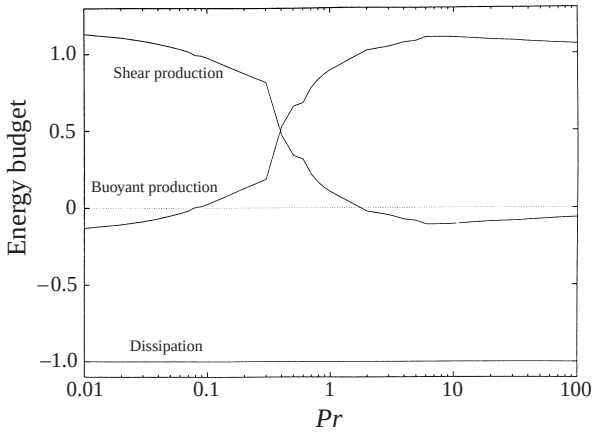


FIGURE 10. Assisted-flow disturbance kinetic energy spectrum, $Re = 1000$.

the stability curve has a jump at a Prandtl number about 0.3. The companion energy budget is shown in figure 10. From the energy budget, it is seen clearly that this jump is due to the shift of the instability mechanism from thermal–shear to assisted-thermal–buoyant. When the instability first becomes assisted-thermal–buoyant, the critical Rayleigh number decreases dramatically with increasing Prandtl numbers. At higher Prandtl numbers, the rate of decrease tapers off. The thermal–shear instability will not disappear completely, though becoming less dominant, until the Prandtl number is greater than around 0.8.

Figure 11 is the projection of the disturbance streamlines for oil in a meridional section, where $Z = \alpha(z - ct)$ is the convective coordinate in $[0, 2\pi]$. It is seen that for Reynolds numbers lower than 35 the disturbances consist of two counter-rotating cells. Increasing the Reynolds number will decrease the size of one of the cells. For Reynolds numbers greater than 40, these two cells will merge together to form a single cell. For flows with Reynolds number greater than 40, the streamlines exhibit the 'cat's eye' pattern, where the mixing is confined to the central portion of the pipe and outside this region the disturbances are upward travelling spiral waves. Similar streamline patterns are also observed for water and oil (Su 1994). Figure 12 illustrates isotherms of the disturbances for oil at selected Reynolds numbers. Like velocity fluctuations, thermal perturbations are also more active in the central region of the pipe.

### 4.5. *Buoyancy-opposed flow stability*

The stability map of buoyancy-opposed flow is shown in figure 13. The first azimuthal mode is again the most unstable. The stability curve is primarily dependent upon the Rayleigh number and only secondarily upon the Prandtl number and Reynolds number. For water, $Ra_c$ is $-120$ at large Reynolds number. Scheele & Hanratty's experiment (1962) was less accurate in measuring the critical $G/R$ for opposed flow since the transition was sudden and sometimes the heat transfer section was not long enough to obtain fully-developed profiles. Nevertheless, they reported that the $G/R$ at transition at all values of $R$ is greater than $-52.2$ ($Ra = -104.4$). At large Reynolds number, the transition $G/R$ appears to approach a constant value of $-59$ ($Ra = -118$). Again, this agrees very well with our numerical value of $-120$. It is worth noting that the basic difference between assisted flow and opposed flow is

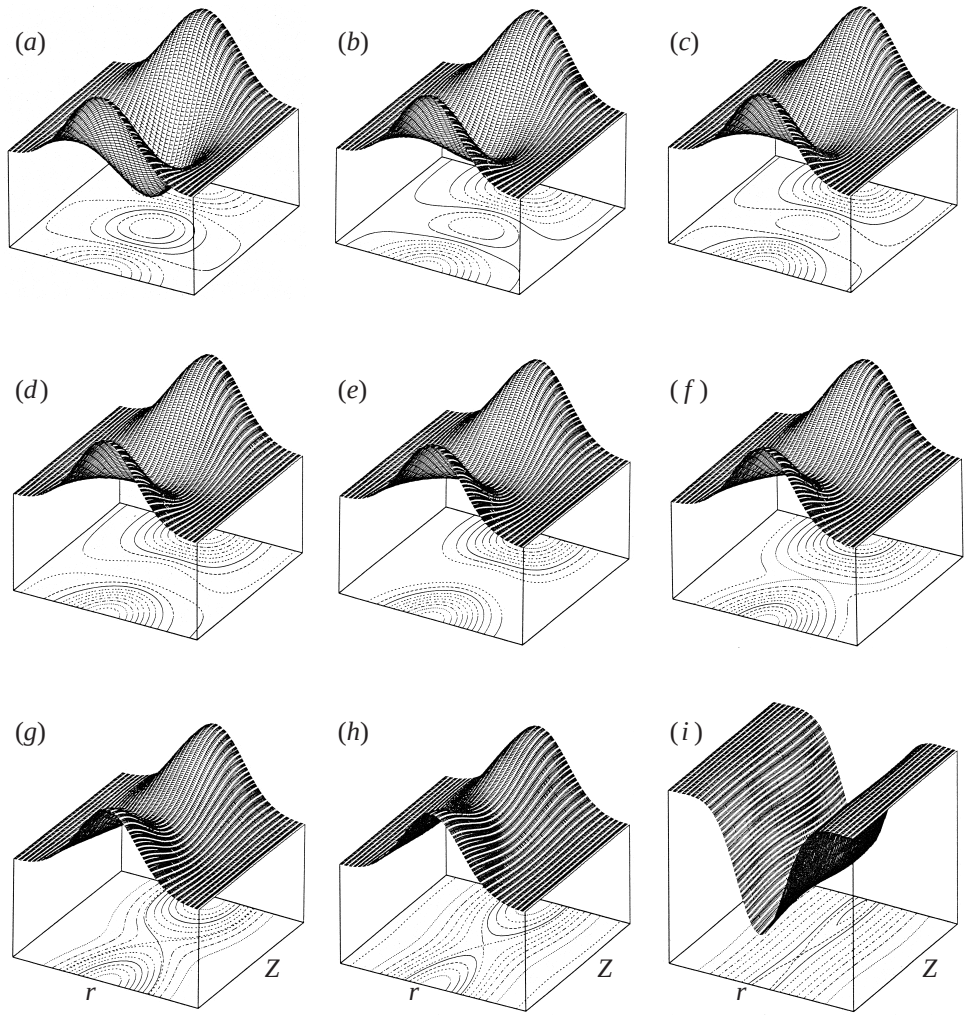


FIGURE 11. The projection of streamlines in a meridional section of the secondary flow at the onset of assisted-flow instability for oil: (*a*) $Re = 10$, (*b*) $Re = 20$, (*c*) $Re = 25$, (*d*) $Re = 30$, (*e*) $Re = 35$, (*f*) $Re = 40$, (*g*) $Re = 60$, (*h*) $Re = 100$, (*i*) $Re = 800$.

that for stagnant fluids assisted flow is stably stratified whereas opposed flow is unstably stratified. Also shown in figure 13 is the *Rayleigh–Taylor* instability. The axial wavenumber of the Rayleigh–Taylor instability is almost zero implying very long, fast travelling instability waves. From figure 13, it is seen that the Rayleigh–Taylor instability occurs at $Ra = -210$ approximately and is independent of the Prandtl number since it is associated with unstable density stratification. The Rayleigh–Taylor instability is dominant only when the Reynolds number is extremely low, lower than about 5. The reason why the Prandtl number does not play a significant role in opposed flow is because the flow is unstably stratified in this setting. For flows with an extremely low speed, the instability takes place because of the Rayleigh–Taylor instability. Increasing the convection will make the flow even more unstable and decrease the magnitude of the critical Rayleigh number. Further increase in the Reynolds number tends to make the critical Rayleigh number approach a constant

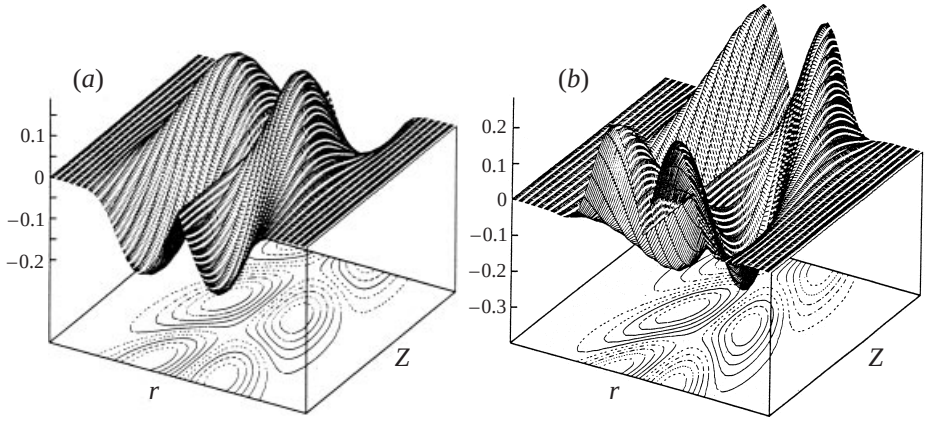


FIGURE 12. The isotherms of the secondary flow at the onset of assisted-flow instability for oil: (*a*) $Re = 20$, (*b*) $Re = 1000$.

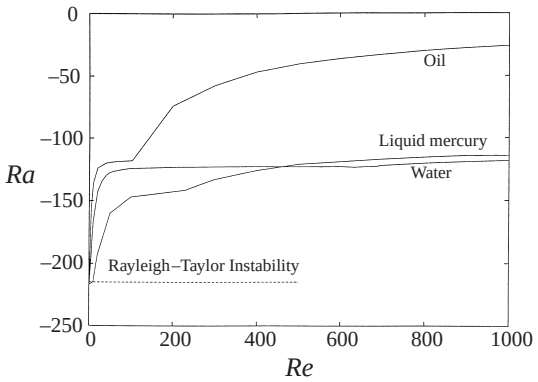


FIGURE 13. Stability map of opposed flow with different Prandtl numbers.

value. The numerical results show that for water the assisted and opposed flows become unstable at $Ra = 66$ and $-120$, respectively, with $Re = 1000$, while the inflection point in assisted flow and flow separation in opposed flow occur at $Ra = 68$ and $-105$, respectively. Such close agreement was also reported in Scheele & Hanratty's experiment (1962), which led them to speculate that assisted flow becomes unstable because the velocity profile develops an inflection point and the opposed flow becomes unstable due to flow separation. However, the present study suggests that their speculation is not completely correct. Figure 5 reveals that the association of inflection point with flow instability is valid only for fluids with Prandtl number equal to or greater than $O(1)$. On the other hand, figure 13 indicates that the attribution of instability to separation is true for fluids with Prandtl number equal to or less than $O(1)$. As a result, Scheele & Hanratty's speculation only applies for fluids with $O(1)$ Prandtl number. Strictly speaking, the appearance of an inflection point and separation are necessary and sufficient conditions for instability in assisted and opposed flows, respectively.

Figure 14 provides the relationship of the critical axial wavenumber and wave speed with the Reynolds number for opposed flow. The variations exhibit quite irregular patterns, common to all three fluids. If the Reynolds number is very close to zero, the wavenumber is virtually zero because the Rayleigh–Taylor instability dominates.

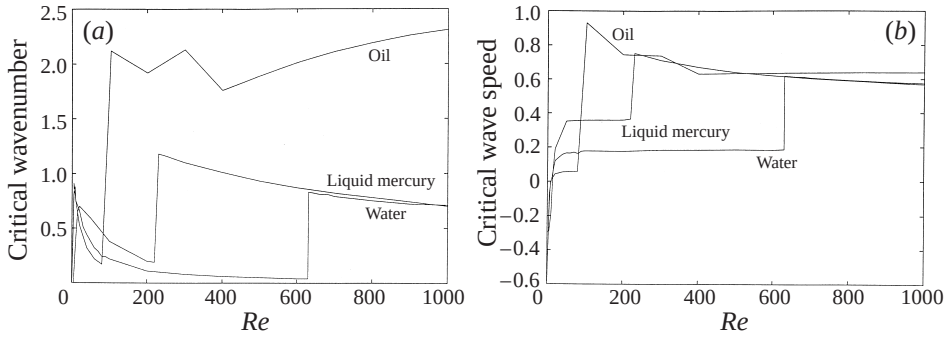


FIGURE 14. (*a*) Critical wavenumber and (*b*) critical wave speed of opposed flow.

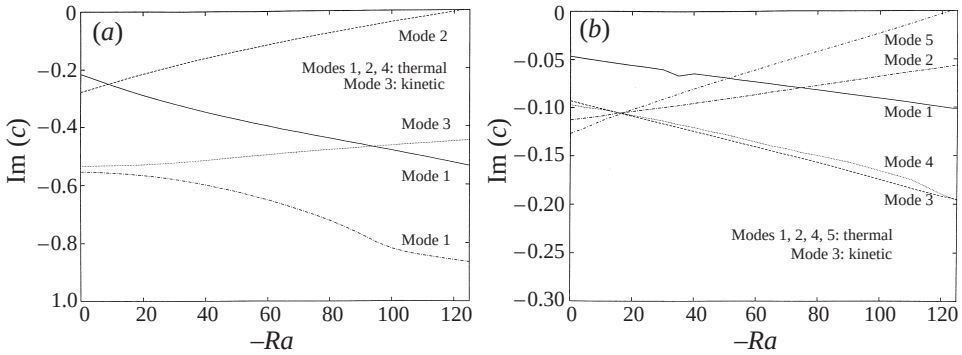


FIGURE 15. Evolution of growth rate with *Ra* for water, opposed flow: (*a*) $Re = 630$, $\alpha = 0.04$; (*b*) $Re = 640$, $\alpha = 0.83$.

A slight increase in the Reynolds number decreases the wavelength substantially since the Rayleigh–Taylor instability is taken over by a different instability. Further increase in convection will result in a smooth decrease in the wavenumber. However, at certain Reynolds numbers, there is a sudden jump in the critical wavenumber. After that, the wavenumber decreases again. This sudden rise in the critical wavenumber is related to another change in the instability mechanism, as discussed later. The critical wave speed also experiences a similar sudden change, as shown in figure 14(*b*). Figure 15 shows the evolution of the growth rate and wave speed with *Ra* before and after the sudden change in the wavenumber for water. The results show that the most unstable modes are triggered by thermal perturbations in either case. Therefore, whether the most unstable mode is a kinetically or thermally induced fluctuation is only determined by the magnitude of the Prandtl number and independent of the instability mechanisms or other factors.

Figure 16 presents the energy budgets for liquid mercury, water and oil, respectively. All three exhibit similar features. At Reynolds numbers below about 5, the disturbances extract energy from the mean flow exclusively by buoyant production and lose it through viscous dissipation. The production from shear is identically zero, i.e. the shear force has nothing to do with the instability. This instability is of the Rayleigh–Taylor type. Increasing the convection effect will increase the shear production. Up to the Reynolds number where the sudden change in the critical wavenumber occurs, as depicted in figure 14, the buoyant production remains the main source of instability. After the sudden change, the shear production becomes dominant. These

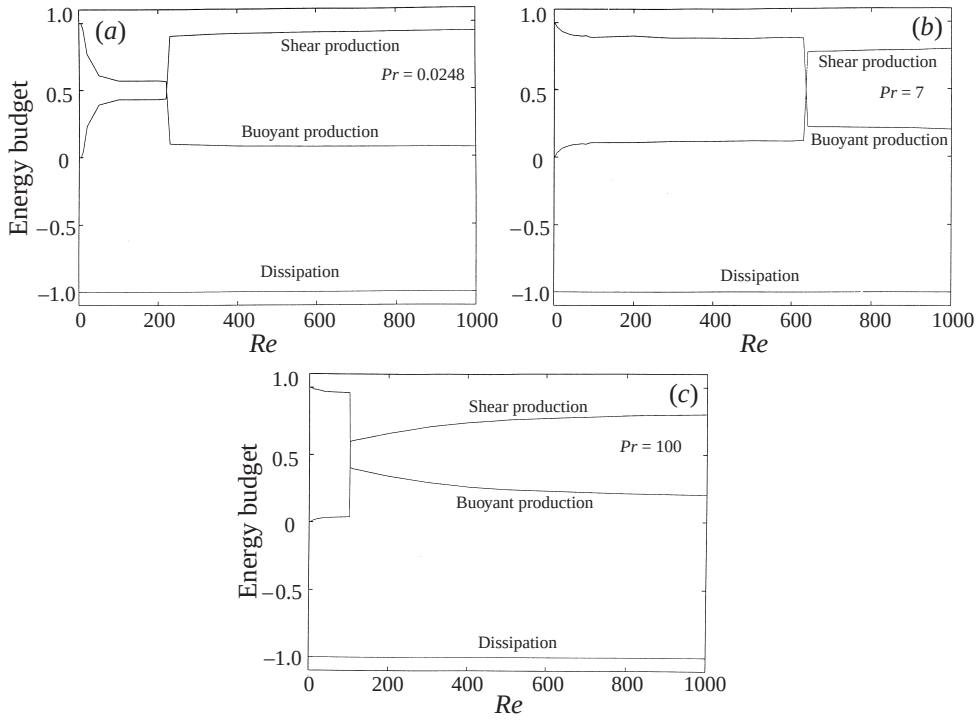


FIGURE 16. Opposed-flow disturbance kinetic energy budget for (*a*) liquid mercury, (*b*) water, (*c*) oil.

two different instability mechanisms are named *opposed-thermal–buoyant* instability and thermal–shear instability. This type of thermal–buoyant instability was also identified by previous investigators (Yao & Rogers 1989; Chen & Chung 1996) in mixed convection flow though they made no distinction in the nature of instability between assisted flow and opposed flow. This difference for the thermal–buoyant instability between assisted and opposed flows is not trivial. Although both instabilities obtain energy from buoyant production, they are quite different in origin. The reason why the Prandtl number effect is significant for assisted flow instability is explained in § 4.3. For opposed-thermal–buoyant instability, the base flow is unstably stratified and instability develops accordingly. The energy of disturbances is supplied from unstable density stratification, not from undamped thermal fluctuations. Thus opposed-thermal–buoyant instability does not depend on the Prandtl number. As a result, the Prandtl number does not play an active role. Increasing the effect of convection finally shifts the instability mechanism to thermal–shear instability. The sudden changes in the critical wavenumber and wave speed shown in figure 14 are associated with the shift of instability from opposed-thermal–buoyant to thermal–shear. Figures 17 and 18 demonstrate the $Pr, Ra$-space stability map and the energy budgets at $Re = 1000$. At this Reynolds number the thermal–shear instability is dominant for all Prandtl numbers.

Figure 19 provides the projection of streamlines at a meridional section for oil at different Reynolds numbers. Figure 19(*a*) presents the case of Rayleigh–Taylor instability. The disturbances are infinite in length and the streamlines are straight in the vertical direction. For $Re \leqslant 103$, before the sudden change in the critical wavenumber occurs, the disturbances are long waves and, as in the assisted flow case,

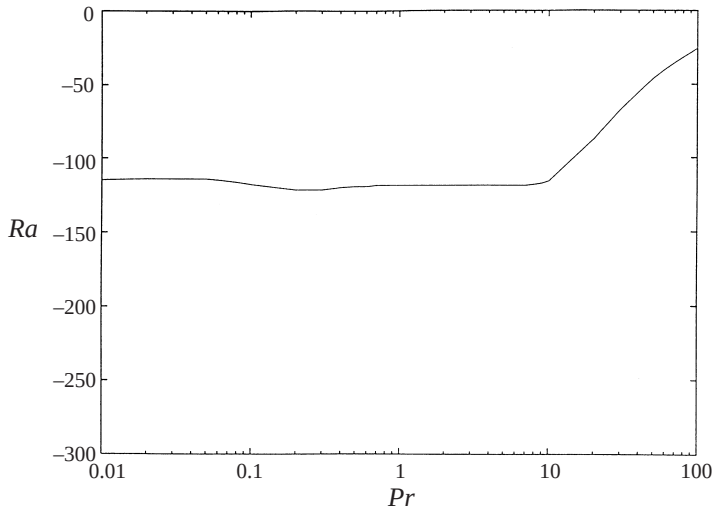


FIGURE 17. Stability map in $Pr, Ra$-space for opposed flow, $Re = 1000$.

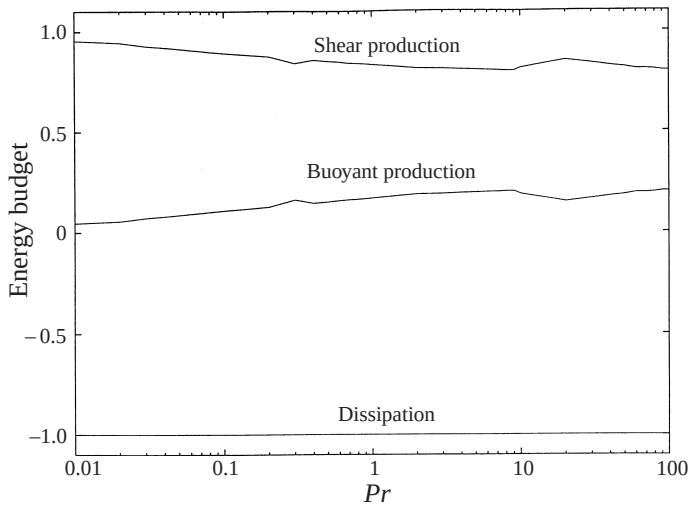


FIGURE 18. Opposed-flow disturbance kinetic energy spectrum, $Re = 1000$.

the streamlines consist of a rotating cell in the centre and travelling waves in the outer portion. For $Re \geqslant 103$, the wavelength becomes shorter and the streamlines are rotating cells. Figure 20 shows the isotherms for oil. Figure 20(*a*) shows isotherms for the Rayleigh–Taylor instability: they are symmetrical and neatly stacked temperature cells because, for the Rayleigh–Taylor instability, the infinitely long waves do not induce local mixing. For lower Reynolds numbers, the isotherms become skewed and slightly overlapped through the spiral modes, as shown in figure 20(*b–c*). For $Re \geqslant 103$, the isotherms, figure 20(*d–g*), are quite irregular. The strong gradients at the pipe centre are a manifestation of thermal–shear instability. Similar patterns were also found by Ali & Weidman (1990) in a circular Couette flow with radial heating.

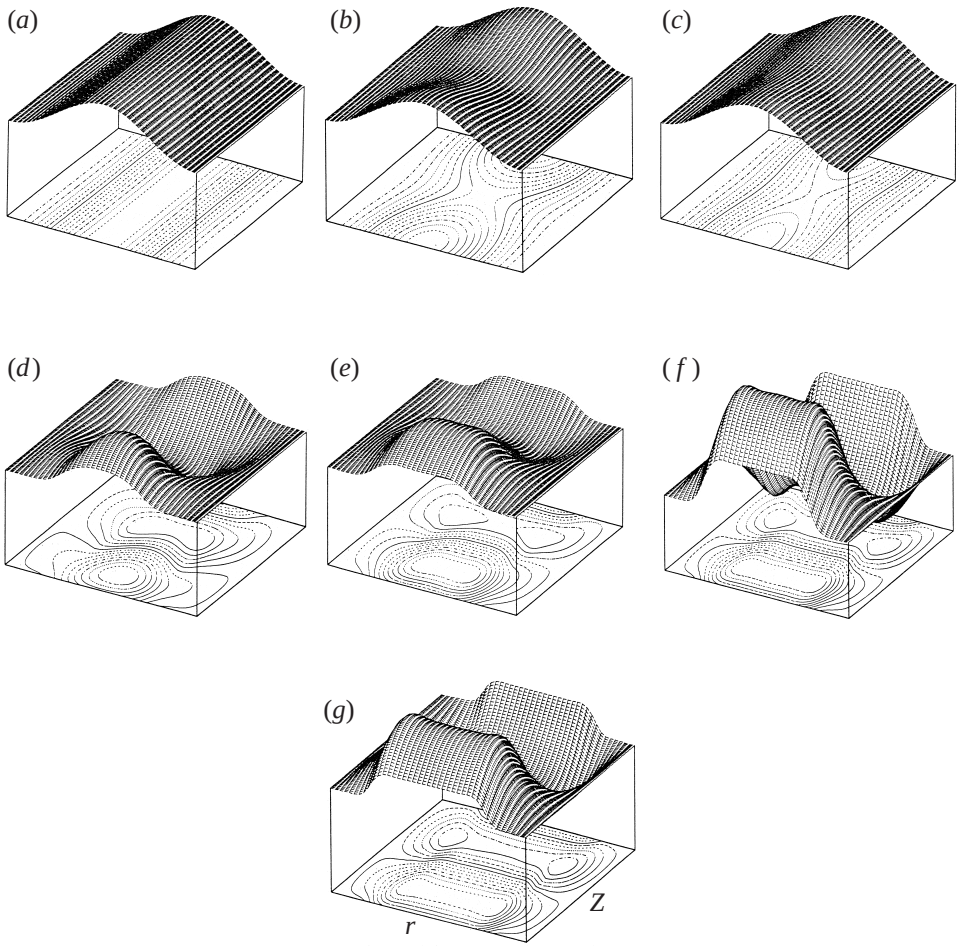


FIGURE 19. The projection of streamlines in a meridional section of the secondary flow at the onset of opposed flow instability for oil: (*a*) Rayleigh–Taylor instability, (*b*) $Re = 40$, (*c*) $Re = 100$, (*d*) $Re = 110$, (*e*) $Re = 200$, (*f*) $Re = 600$, (*g*) $Re = 1000$.

## 5. Conclusion

A primitive-variable formulation of the governing equations together with the Chebyshev collocation method has been used to study the stability of mixed convection flow in a vertical pipe. This is in contrast to the standard approach of reducing the governing equations to a set of higher-order differential equations. While this formulation requires somewhat higher computer storage for eigenvalue calculation using the QR algorithm, it is easily adaptable to various flow situations. The Chebyshev collocation method yields fast and accurate results with moderate computation time in the present study.

The linear stability analysis of mixed convection flow in a vertical pipe indicates that non-isothermal flow can be highly unstable at low Reynolds number and Rayleigh number. The predicted values of the critical Rayleigh number for water are in excellent accord with the experimental measurement of Scheele & Hanratty (1962). The unstable wave is a double spiral travelling wave. The instability mechanisms for buoyancy-assisted flow are significantly different from those for buoyancy-opposed

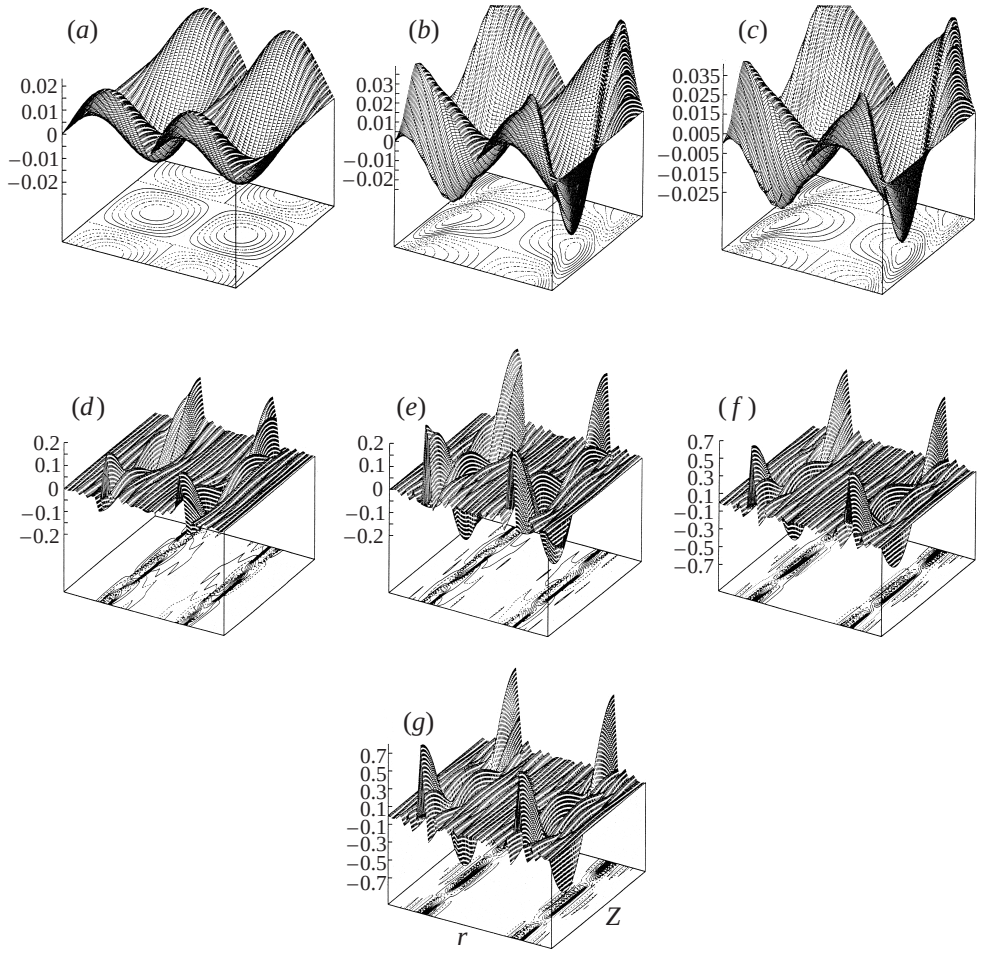


FIGURE 20. The isotherms of the secondary flow at the onset of opposed flow instability for oil: (*a*) Rayleigh–Taylor instability, (*b*) $Re = 40$, (*c*) $Re = 100$, (*d*) $Re = 110$, (*e*) $Re = 200$, (*f*) $Re = 600$, (*g*) $Re = 1000$.

flow. The Prandtl number plays an integral role in assisted-flow instability but less so in opposed flow. There are two instability mechanisms in the assisted flow: thermal–shear instability for flows with Prandtl numbers less than 0.3 and assisted-thermal–buoyant instability for flows whose Prandtl numbers are greater than 0.3. For opposed flow, the Prandtl number effect is less important and there are three instability mechanisms: the Rayleigh–Taylor instability for flows with extremely low Reynolds numbers ($Re \leqslant 5$); at somewhat larger Reynolds numbers the opposed-thermal–buoyant instability is dominant; and the thermal–shear instability arises at higher Reynolds numbers. The instability in assisted and opposed flows can be attributed to the appearance of an inflection point and flow separation for fluids with Prandtl number $O(1)$. Since velocity and temperature fields of the constant wall temperature case are governed by similar types of equations as constant flux heating, the results reported here are applicable qualitatively to the heated vertical pipe with constant wall temperature.

The present work gives a generic picture of the linear stability characteristics of mixed convection in a vertical pipe. It is speculated that transition mechanisms in

non-isothermal flow are likely to be very different from those in isothermal flows. Any analysis of mixed convection flow based on the fully-developed approximation cannot be justified unless a stability study indicates otherwise. Non-isothermal flow undergoes transition at very low Reynolds numbers and Rayleigh numbers so heating alters the transition scenarios substantially. Although several different transition routes to turbulence have been well established for isothermal flow, as outlined by the Morkovin map (Panton 1996), there remains much to be done to make a non-isothermal version of the Morkovin map a reality.

## REFERENCES


Abramowitz, M. & Stegun, I. A. 1972 *Handbook of Mathematical Functions*. Dover.

Ali, M. & Weidman, P. D. 1990 On the stability of circular Couette flow with radial heating. *J. Fluid Mech.* **220**, 53–84.

Batchelor, G. K. & Gill, A. E. 1962 Analysis of the stability of axisymmetric jets. *J. Fluid Mech.* **14**, 529–551.

Canuto, C., Hussaini, M. Y., Quarteroni A. & Zang, T. A. 1988 *Spectral Methods in Fluid Dynamics*. Springer.

Chen, Y.-C. & Chung, J. N. 1996 The linear stability of mixed convection in a vertical channel. *J. Fluid Mech.* **325**, 29–51.

Davey, A. & Drazin, P. G. 1969 The stability of Poiseuille flow in a pipe. *J. Fluid Mech.* **36**, 209–218.

Davey, A. & Nguyen, H. P. F. 1971 Finite-amplitude stability of pipe flow. *J. Fluid Mech.* **45**, 701–720.

Drazin, P. G. & Reid, W. H. 1981 *Hydrodynamic Stability*. Cambridge University Press.

El-Genk, M. S. & Rao, D. V. 1990 Buoyancy induced instability of laminar flows in vertical annuli – I: Flow visualization and heat transfer experiments. *Intl J. Heat Mass Transfer* **33**, 2145–2159.

Fox, J. A., Lessen, M. & Bhat, W. V. 1968 Experimental investigation of the stability of Hagen–Poiseuille flow. *Phys. Fluids* **11**, 1–4.

Gary, J. & Helgason, R. 1970 A matrix method for ordinary differential eigenvalue problems. *J. Comput. Phys.* **5**, 169–187.

Gebhart, B., Jaluria, Y, Mahajan, R. L. & Sammakia, B. 1988 *Buoyancy-Induced Flows and Transport*. Hemisphere.

Hanratty, T. J., Rosen, E. M. & Kabel, R. L. 1958 Effect of heat transfer on flow field at low Reynolds numbers in vertical tubes. *Indust. Engng Chem.* **50**, 815–820.

Kemeny, G. A. & Somers, E. V. 1962 Combined free and forced convection on stability flow in vertical circular tubes. *J. Heat Transfer* **84**, 339–346.

Khorrami, M. R., Malik, M. R. & Ash, R. L. 1989 Application of spectral collocation techniques to the stability of swirling flows. *J. Comput. Phys.* **81**, 206–229.

Landahl, M. T. 1975 Wave breakdown and turbulence. *SIAM J. Appl. Math* **28**, 735–756.

Landau, L. D. & Lifshitz, E. M. 1959 *Fluid Mechanics*. Pergamon.

Lessen, M., Sadler, S. G. & Liu, T. Y. 1968 Stability of pipe Poiseuille flow. *Phys. Fluids* **11**, 1404–1409.

Maitra, D. & Raju, K. S. 1975 Combined free and forced convection laminar heat transfer in a vertical annulus. *J. Heat Transfer* **97**, 135–137.

Moler, C. B. & Stewart, G. W. 1973 An algorithm for generalized matrix eigenvalue problems. *SIAM J. Numer. Anal.* **10**, 241–256.

Orszag, S. A. 1971 Accurate solution of the Orr–Sommerfeld stability equation. *J. Fluid Mech.* **50**, 689–703.

Panton, R. L. 1996 *Incompressible Flow*. John Wiley & Sons.

Reynolds, W. C. & Potter, M. C. 1967 Finite-amplitude instability of parallel shear flow. *J. Fluid Mech.* **27**, 465–492.

Rogers, B. B. & Yao, L. S. 1993 The importance of Prandtl number in mixed-convection instability. *J. Heat Transfer* **115**, 482–486.

Rosen, E. M. & Hanratty, T. J. 1961 Use of boundary-layer theory to predict the effects of heat

transfer on the laminar-flow field in a vertical tube with a constant-temperature wall. *J. AIChE* **7**, 112–123.

Salwen, H., Cotton, F. W. & Grosch, C. E. 1980 Linear stability of Poiseuille flow in a circular pipe. *J. Fluid Mech.* **98**, 273–284.

Scheele, G. F. & Hanratty, T. J. 1962 Effect of natural convection on stability of flow in a vertical pipe. *J. Fluid Mech.* **14**, 244–256.

Su, Y. C. 1994 Linear stability analysis of mixed convection flow in a vertical pipe. MS Thesis, Washington State University.

Su, Y. C., Wang, C. S., Chung, J. N. & Lee, S. T. 2000 An accurate method for the simulation of three-dimensional incompressible heated pipe flow. *Numer. Heat Transfer*. B **37**, 293–308.

Yao, L. S. 1987*a* Is a fully-developed and non-isothermal flow possible in a vertical pipe? *Intl. J. Heat Mass Transfer* **30**, 707–716.

Yao, L. S. 1987*b* Linear stability analysis for opposed mixed convection in a vertical pipe. *Intl J. Heat Mass Transfer* **30**, 810–811.

Yao, L. S. & Rogers, B. B. 1989 The linear stability of mixed convection in a vertical annulus. *J. Fluid Mech.* **201**, 279–298.